

CHARACTERISTICS OF WAVE PROPAGATION AND ENERGY DISTRIBUTIONS IN CYLINDRICAL ELASTIC SHELLS FILLED WITH FLUID

C. R. FULLER AND F. J. FAHY

Institute of Sound and Vibration Research, University of Southampton, Southampton SO9 5NH, England

(Received 16 March 1981, and in revised form 10 August 1981)

The dispersion behaviour and energy distributions of free waves in thin walled cylindrical elastic shells filled with fluid are investigated. Dispersion curves are presented for a range of parameters and the behaviour of individual branches is explained. A non-dimensional equation which determines the distribution of vibrational energy between the shell wall and the contained fluid is derived and its variation with frequency and material parameters is studied.

1. INTRODUCTION

The problems of elastic wave propagation in thin walled shells *in vacuo* and in fluid contained in rigid cylindrical ducts have separately received a great deal of attention. When the two fields are coupled together, by allowing the duct wall to be elastic, the resulting wave behaviour is far more complex and consequently there is less literature available on this topic. In particular, little physical explanation of the behaviour of waves in terms of propagation and energy distribution through the shell system has been attempted.

Nearly a century ago, Lamb [1] produced a comprehensive analysis of the influence of wall compliance on wave propagation in tubes, but he dismissed flexural waves as being of little importance. Much previous work [2–4] has been concerned solely with propagating waves of an axisymmetric nature. Various approximations such as a restriction to low frequencies or ignoring the Poisson's coupling of the shell have been made in these analyses. Thomson [5] introduced the effects of Poisson's ratio and included flexural and axial wave motion and evaluated the phase velocities of the first three axisymmetric "fluid" waves. Lin and Morgan [6] have studied the propagation of axisymmetric waves through fluid contained in an elastic cylindrical shell. In their analysis they treated the dependence of phase velocity on various physical parameters of the system without the approximations introduced by previous authors: however, their results are limited to real wave numbers and to circumferential modes of zero order.

More recently Kumar [7] has investigated the dispersion of waves in fluid-filled shells by using exact elastic equations valid for shells of any wall thickness. Results were presented for the real, imaginary and complex parts of the wavenumber domain but are restricted to axisymmetric waves and relatively thick shells. One reviewer has drawn our attention to the fact that Kumar's analysis is in error in suggesting that the quasi-plane mode in thin shells displays the cut-off phenomenon at the ring resonance, an error which results from neglect of higher order terms, including the flexural rigidity term, in a power series expansion in thickness-radius ratio. The problem of excitation of normal

modes by a point source located in the fluid contained in an elastic cylindrical shell has been considered by Merkulov *et al.* [8]. Dispersion curves, limited to the real and imaginary planes and a relatively thick shell, were presented for modes of circumferential order, $n = 0, 1$ and 2 .

The purpose of the present paper is to investigate more completely the dispersion and energy distributions of waves in fluid-filled shells of cylindrical cross-section. Dispersion curves for waves of circumferential order $n = 0$ and $n = 1$ are derived and branches in the real, imaginary and complex planes are found. Variation of shell wall thickness and material is considered and the results discussed with the aim of attaching some physical significance to the wave behaviour in terms of the various system parameters.

Finally, a non-dimensional equation is derived which determines the distribution of vibrational energy between the fluid and the shell wall for a particular mode, and the variation of the energy ratio with frequency and system parameters is discussed. Previous studies on energy sharing in fluid-filled cylindrical shells include approximate analyses by Fay *et al.* [2], Jacobi [3] and more recently White [9]. All these analyses are limited to axisymmetric modes and only radial motion of the shell with no Poisson's coupling is considered. This approximation introduces a large error, as for certain waves or frequency regions a high amount of energy may be carried by axial or tangential extension of the shell wall. White's analysis is extended to higher frequencies by using a statistical energy approach which obscures some important characteristics of the energy distribution behaviour.

Thomson [5] included Poisson effects and axial motion and evaluated the ratios of energy flux in the shell and fluid; however he considered only radial velocity and shear and apparently ignored the contributions of bending moment and axial force.

The study presented in this paper was carried out as a preliminary stage in an analysis of wave transmission and reflection at discontinuities in fluid-filled pipes which will be presented in a companion paper.

2. EQUATIONS OF MOTION OF THE COUPLED SYSTEM

The co-ordinate system and circumferential mode shapes used in this analysis are shown in Figure 1. The free, simple harmonic motion of a thin-walled cylindrical shell containing an acoustic field can be most conveniently described by the Donnell–Mushtari shell equations [10]. These equations are valid for thin walled shells and exclude the effects of rotary kinetic energy and transverse shear. The normal mode shapes assumed for the displacements of the shell wall, associated with an axial wavenumber k_{ns} , are

$$u = \sum_{s=0}^{\infty} \sum_{n=0}^{\infty} U_{ns} \cos(n\theta) \exp[i\omega t - ik_{ns}x + i\pi/2], \quad (1a)$$

$$v = \sum_{s=0}^{\infty} \sum_{n=0}^{\infty} V_{ns} \sin(n\theta) \exp[i\omega t - ik_{ns}x], \quad (1b)$$

$$w = \sum_{s=0}^{\infty} \sum_{n=0}^{\infty} W_{ns} \cos(n\theta) \exp[i\omega t - ik_{ns}x]. \quad (1c)$$

The assumed form of the pressure field in the contained fluid which satisfies the acoustic wave equation in cylindrical co-ordinates is

$$p = \sum_{s=0}^{\infty} \sum_{n=0}^{\infty} P_{ns} \cos(n\theta) J_n(k'_s r) \exp[i\omega t - ik_{ns}x]. \quad (2)$$

Substitution of these forms into the shell equations results in the equations of motion

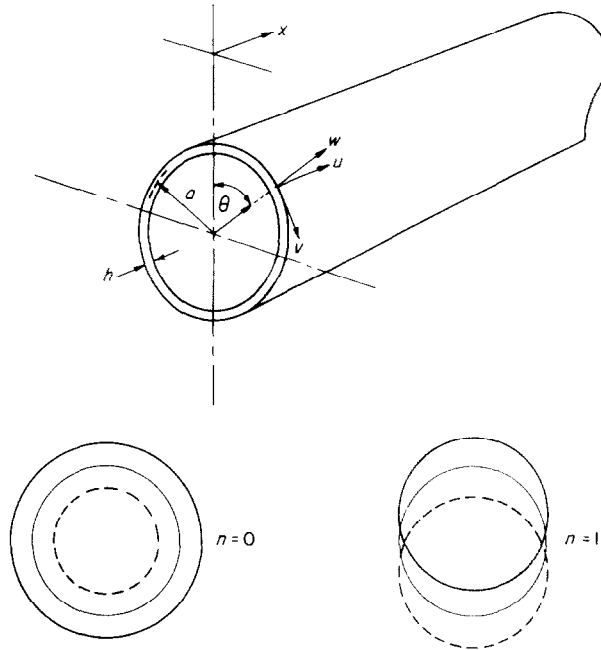


Figure 1. Co-ordinate system and modal shapes.

of the coupled system in terms of the amplitudes of the three displacements and the acoustic pressure. In equations (1) and (2), n is the circumferential modal order, k_{ns} and k'_s are the axial and radial wave numbers respectively, and subscript s denotes a particular branch of the dispersion curves. (A list of symbols is given in the Appendix.)

The motion of the system can thus be represented in matrix form. However before this is done it is convenient to apply the boundary condition at the shell wall. To ensure that the fluid remains in contact with the shell wall the radial fluid vibrational velocity and the shell radial velocity must be equal. Thus for a particular mode (n, s) the radial velocity of the fluid at the shell wall, given by the momentum equation, is

$$v_r|_{r=a} = -\left(\frac{1}{i\rho_f\omega}\right) \partial p/\partial r = -\frac{k'_s J'_n(k'_s a)}{i\rho_f\omega} P_{ns} \cos(n\theta) \exp[i\omega t - ik_{ns}x], \quad (3, 4)$$

where ρ_f is the density of the fluid, a is the radius of the shell, and a prime denotes differentiation with respect to the argument $k'_s r$. Equating $v_r (r = a)$ to the shell radial velocity derived from equation (1c) enables the fluid pressure amplitude to be written in terms of the shell radial displacement amplitude as

$$P_{ns} = [\omega^2 \rho_f / k'_s J'_n(k'_s a)] W_{ns}. \quad (5)$$

The free vibrations of the coupled system can now be represented in matrix form as

$$\begin{bmatrix} L_{11} & L_{12} & L_{13} \\ L_{21} & L_{22} & L_{23} \\ L_{31} & L_{32} & L_{33} \end{bmatrix} \begin{bmatrix} U_{ns} \\ V_{ns} \\ W_{ns} \end{bmatrix} = \begin{bmatrix} 0 \\ 0 \\ 0 \end{bmatrix}, \quad (6)$$

$$L_{11} = -\Omega^2 + (k_{ns}a)^2 + \frac{1}{2}(1-\nu)n^2, \quad L_{12} = \frac{1}{2}(1+\nu)n(k_{ns}a), \quad L_{13} = \nu(k_{ns}a), \quad (7a-c)$$

$$L_{21} = L_{12}, \quad L_{22} = -\Omega^2 + \frac{1}{2}(1-\nu)(k_{ns}a)^2 + n^2, \quad L_{23} = n, \quad (7d-f)$$

$$L_{31} = L_{13}, \quad L_{32} = L_{23}, \quad L_{33} = -\Omega^2 + 1 + \beta^2[(k_{ns}a)^2 + n^2] - FL. \quad (7g-i)$$

In equations (7), Ω is the non-dimensional frequency, $\Omega = \omega a / c_L$, c_L is the extensional phase speed of the shell material, ν is the Poisson's ratio of the shell material and β is the shell thickness parameter given by $\beta^2 = h^2 / 12a^2$. FL is the fluid loading term due to the presence of the fluid acoustic field.

The equations governing the motion of the coupled system are seen to differ from those governing the motion of a shell vibrating *in vacuo* [10] by the presence of a fluid loading term in the element L_{33} of the diagonal of the matrix in equation (6). This fluid loading term is given by

$$FL = \Omega^2 (\rho_f / \rho_s) (h/a)^{-1} (k'_s a)^{-1} [J_n(k'_s a) / J'_n(k'_s a)], \quad (8)$$

where ρ_s is the volume density of the shell material and h is the thickness of the shell.

The radial fluid wavenumber $k'_s a$ is related to the axial wavenumber $k_{ns} a$ by the usual vector relation, written in terms of the shell non-dimensional frequency Ω as

$$k'_s a = \pm [\Omega^2 (c_L / c_f)^2 - (k_{ns} a)^2]^{1/2}, \quad (9)$$

where c_f is the free wave speed in the fluid.

Equation (8) provides immediate insight into the effect of the contained fluid on the shell response. Variation of the fluid loading term can be seen to directly influence the behaviour of the system. At very low frequencies ($\Omega \rightarrow 0$) the fluid loading term is small for shell waves and thus one would expect the fluid-filled shell response to be close to that of an *in vacuo* shell. Similarly when $J'_n(k'_s a) = 0$, the boundary condition for a rigid walled duct mode, the fluid loading term is large and the system behaviour will approach that of an acoustic wave in a rigid walled tube. The variation of FL with radial wavenumber, in a steel shell of thickness $h/a = 0.05$ filled with water for $\Omega = 1$, shown in Figure 2 for $n = 0$ and $n = 1$ illustrates this behaviour. The fluid loading term is either extremely large or relatively small implying that the behaviour of the coupled system will be close to duct modes in some regions of the wavenumber domain and close to *in vacuo* shell modes in others. Equation (8) also predicts that increasing the shell thickness or decreasing the density ratio, ρ_f / ρ_s , decreases the effect of the contained fluid on the shell response and leads to a decrease in the coupling of the shell and fluid behaviour. It is interesting

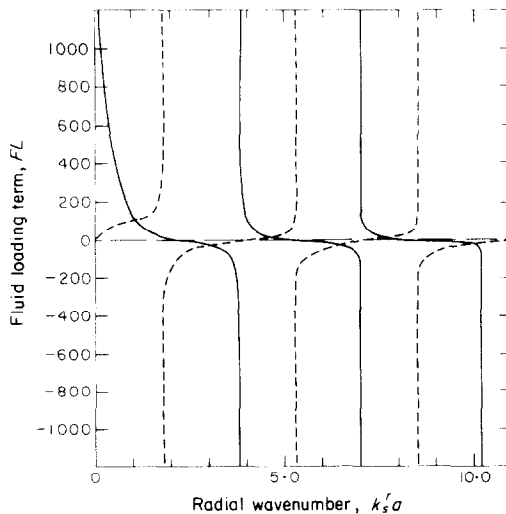


Figure 2. Variation of the fluid loading term with radial wavenumber in a water-filled steel shell, $h/a = 0.05$, $\Omega = 1$; —, $n = 0$; ---, $n = 1$. N.B. sign reversed for $n = 0$.

to note that Figure 2 also represents the general variation in reactive wall impedance, $Z = -i\rho_f\omega J_n(k'_s r)/k'_s J'_n(k'_s r)$, with radial wavenumber. Thus when Z is large, as at the particular values of $k'_s a$ shown in Figure 2, the shell wall will appear as a rigid tube to the fluid.

3. SOLUTION OF THE DISPERSION EQUATION

For a free motion solution to exist the determinant of the amplitude coefficients given by equation (6) must be equal to zero. Expansion of the determinant provides the system characteristic equation. In the case of the *in vacuo* shell the characteristic equation can be written in polynomial form and thus readily solved [11]. With the inclusion of fluid loading, the characteristic equation of the coupled system is "non-linear" due to the presence of the desired eigenroots in the argument of the Bessel functions of the fluid loading term and numerical methods have to be used to find the roots of the equation.

The roots of the characteristic equation were found, once approximately located, by using a complex root searching technique based on Newton's rule [12], adapted for use on an ICL 2900 computer. For the cases of purely real or imaginary values of axial wavenumber the approximate locations were readily found by using a simple stepping procedure to locate a change in sign of the characteristic equation. Singularities of the characteristic function were eliminated by noting that where these occurred, the fluid loading term changed sign.

Due to the four dimensional nature of the complex domain, the complex roots are far more difficult to find. A contour integration technique, as used by Kumar and Stephens [13], provides an elegant method of finding the approximate location of the root; however this method requires a large amount of computing time. A simpler and quicker method suitable for cylindrical shells was developed by using the *in vacuo* shell dispersion results at low frequencies. Use of the *in vacuo* bending near field [11], as an approximate initial value in the search for complex roots in relatively thick shells ($h/a \geq 0.01$), was found to lead to quick location of the roots. For relatively thin shells ($h/a \leq 0.01$) the *in vacuo* bending near field was used as an initial value at low frequencies ($\Omega < 0.4$). Above this frequency the root obtained at the previous frequency of interest was taken as the initial value.

TABLE 1
Material properties

Material	Young's modulus (N/m ²)	Poisson's ratio	Density (kg/m ³)	Free wave speed (m/s)
Steel	19.2×10^{10}	0.30	7800	5200
Hard rubber	0.19×10^{10}	0.4	1100	1450
Water	—	—	1000	1500

Dispersion curves were obtained for different shells made from steel or hard rubber filled with water, the properties of which are given in Table 1. Results are presented for circumferential modes of $n = 0$ and $n = 1$; together these modes exhibit all the general characteristics of waves propagating in fluid-filled shells. In Figures 3–8 the complex branches are represented by plotting the real and imaginary parts separately in the real and imaginary planes as dashed lines. For the branch $s = 6$ the real part is negative in value.

4. RESULTS

4.1. STEEL SHELL OF THICKNESS $h/a = 0.05$ VIBRATING IN THE BREATHING MODE ($n = 0$)

Figure 3 shows the dispersion curves of axial wavenumber versus non-dimensional frequency obtained for waves of circumferential order $n = 0$, or the breathing mode, for free waves in a water filled steel shell of thickness $h/a = 0.05$. Various cylindrical duct modes with either a pressure release or a rigid boundary are also plotted for comparison. The $n = 0$ torsional shell mode has been omitted from Figure 3 as it is uncoupled from all other motions.

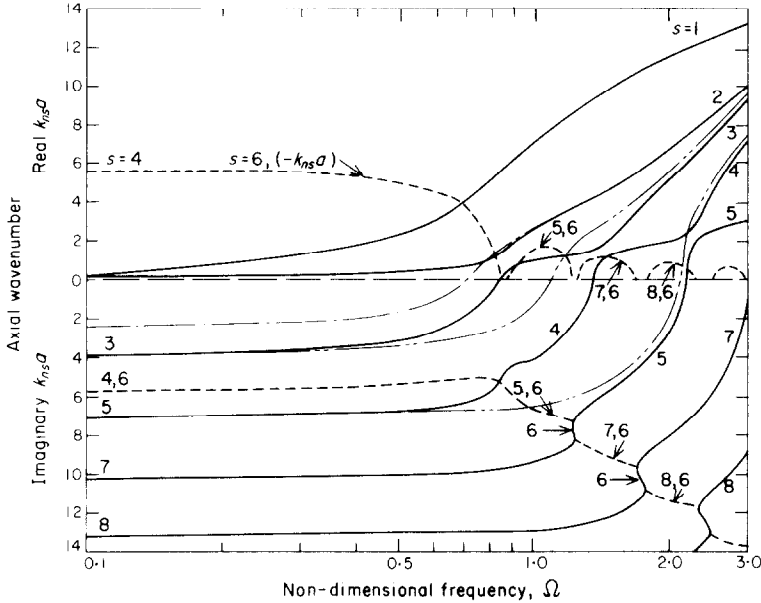


Figure 3. Dispersion curves for a water-filled steel shell of thickness $h/a = 0.05$, $n = 0$; —, purely real and imaginary $k_{ns}a$; ---, real and imaginary parts of complex $k_{ns}a$; - · - ·, pressure release duct solution; - - - -, rigid walled duct solution.

The real branches will be discussed first. As found by previous workers [6–8], two branches exist at low frequencies. The first branch, $s = 1$, is close to a fluid wave in a rigid walled tube. The shell appears very rigid at low frequencies due to its inability to undergo radial motion of long axial wavelength. The second branch, $s = 2$, is close to the *in vacuo* shell wave at low frequencies. Previous work [11] has shown this wave to have very small radial amplitude of vibration, and it is thus largely unaffected by the presence of the fluid. As the frequency is increased the shell resonates as a ring ($\Omega \approx 0.8$) and the shell and fluid motions become strongly coupled. The first branch approaches the *in vacuo* flexural solution. The second branch, $s = 2$, approaches the first pressure release duct mode. This behaviour is due to a rapid increase in radial vibration of the shell and a corresponding increase in coupling with the fluid.

A third branch, $s = 3$, can be seen, from Figure 3, to cut on at $\Omega = 0.85$. Initially this branch closely follows that of the corresponding extensional *in vacuo* shell wave until at $\Omega \approx 1.3$ it turns sharply to approach the second rigid walled acoustic mode. Near this frequency a fourth branch, $s = 4$, cuts on as a fluid wave in a tube with compliant walls and then turns into a plateau to change its behaviour to that of an extensional shell wave largely uncoupled from the fluid. Similarly all higher branches cut on as fluid waves and

then quickly change their behaviour to that of shell waves while the previous shell type branch converts to a fluid wave: at higher frequencies cut-on occurs near rigid walled duct cut-on frequencies. Under no conditions do branches cross in the real plane.

This complex behaviour can be explained by considering the coincidence of an extensional shell wave and a fluid wave in a duct with slightly compliant walls. At the point where one branch enters a plateau and the other branch leaves it, free motion can exist independently both in the fluid and the shell wall. The shell vibrates largely as *in vacuo* due to the extensional nature of the motion and correspondingly the tube appears very rigid to the fluid. However due to the Poisson's effect there is some slight coupling between the shell and fluid motion. As the frequency is increased along a plateau to the position of coincidence of free shell and fluid waves the "forced" pressure field subsequently encounters a fluid free propagation region and the system behaviour changes to a fluid type wave. Similarly the "forced" shell wave for the next branch encounters a shell free propagation region at the same coincidence point and its behaviour changes to that of a shell wave.

A consideration of group velocity (proportional to the inverse slope of the dispersion curve) demonstrates why branches cannot cross. If the branches did cross at coincidence then the fluid and shell motions, although having an equal energy of vibration (see later), would have different rates of propagation of energy, a situation that clearly could not exist. It is interesting to note that even in air-filled steel shells the branches will have plateaux and will not cross. However in this case the corners will be so sharp as to be indiscernible.

In the purely imaginary plane of Figure 3 the wavenumber solutions at low frequencies are almost identical to rigid walled duct modes below cut-off due to the rigidity of the shell wall at low frequencies. Hence there will be an infinite number of branches corresponding to modes with an increasing number of radial nodes. As the frequency is increased the shell becomes less stiff in the radial direction and the branches fall between the rigid walled and pressure release solutions for a cylindrical duct. The purely imaginary branches for the system under discussion, with a relatively thick wall, can be seen from Figure 3 to be characterized by "meanders" which appear in the branch above the ring frequency. At first inspection it appears that at these "meanders" a branch may be multi-valued for a single frequency as shown in the results of Merkulov *et al.* [8]. This condition would contravene the assumed Fourier solution of individual modes with separable co-ordinates. However with the inclusion of the complex wavenumber solutions, each branch below cut-off can be correctly identified and shown to obey the assumed form of solution.

The complex branches, plotted in Figure 3 as broken lines, at low frequencies, are very close to those obtained for an *in vacuo* shell for reasons discussed previously in section 2. At zero frequency the two branches, $s = 4$ and 6, have non-zero complex values of the same absolute magnitude, with the real parts of opposite sign which reduce with increasing frequency to meet the imaginary plane at the same point. No complex branches occur for duct type waves at low frequencies. As discussed in reference [11] complex branches occur in combinations of $\pm(\psi \pm i\phi)_{ns}$ and the pair that represent wave motion in the positive x direction are $(\pm\psi - i\phi)_{ns}$ which together form an attenuated standing wave in the axial direction along the shell wall. Similarly the radial wavenumbers, related to the axial wavenumbers by equation (9), will exist in corresponding (to the axial wavenumber) pairs of $(\beta \pm i\eta)_{ns}$ for the positive direction of propagation. Now, a Bessel function of complex argument has no zeros, and thus individually the complex branches would represent evanescent motion with no radial nodes in the fluid field. When the two radial wavenumbers are considered together they represent two waves of

equal magnitude whose phase varies in an opposite sense with an increase in radial position and which thus combine together to form an interference pattern with radial nodes across a cross section of the contained fluid. The interference pattern amplitude decays inwardly from the shell wall and is zero at $r = 0$.

At high frequencies the complex branches are seen from the results of Figure 3 to provide branch links which leave the imaginary plane (with opposite sign of the real part) at the peak of a "meander" and re-enter the imaginary plane at the rear of the next "meander". Thus, typically a fluid-type branch is imaginary at low frequencies, near the occurrence of a "meander" becomes complex over a small frequency range, becomes purely imaginary near the next "meander", and eventually cuts on. Likewise a branch which is close to the *in vacuo* bending near field shell branch is complex at low frequencies and progresses with increasing frequency as shown in Figure 3 (branch $s = 6$) as a series of complex and imaginary sections. If the shell wall thickness is increased or the density of contained fluid decreased, the "meanders" become sharper, the real part of the complex solutions are reduced in magnitude, and the branch, $s = 6$, approaches the corresponding *in vacuo* bending near field discussed in reference [11]. At the same time the fluid-type parts of the other branches approach rigid walled duct modes below cut-off. The paired complex branches, for example $s = 7$ and 6, would thus appear in the light of the results to correspond to near field coincidence behaviour between shell and duct waves below cut-off.

4.2. STEEL SHELL OF THICKNESS $h/a = 0.05$ VIBRATING IN THE BEAM MODE ($n = 1$)

Dispersion curves for a cylindrical fluid-filled shell with identical material parameters to those in section 4.1, vibrating in the circumferential mode of order $n = 1$, or the beam mode, are presented in Figure 4. The dispersion curves exhibit behaviour similar to that discussed for the breathing mode, apart from a few major differences. There exists at low frequencies (for the $n = 1$ mode) only one branch, $s = 1$, which corresponds to the beam type shell motion [11]. This wave is acoustically "slow": that is, its radial wavenum-

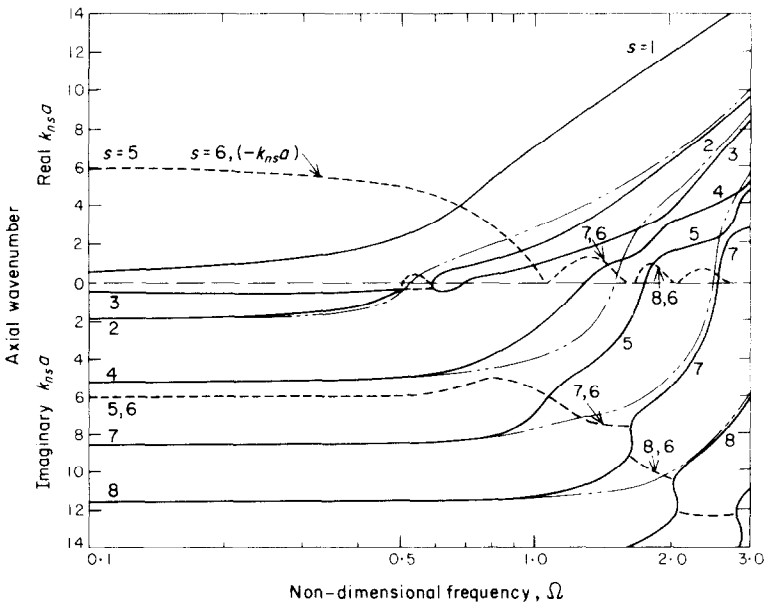


Figure 4. Dispersion curves for a water-filled steel shell of thickness $h/a = 0.05$, $n = 1$; —, purely real and imaginary $k_{ns}a$; - - -, real and imaginary parts of complex $k_{ns}a$; - - - - -, rigid walled duct solution.

ber is imaginary and hence the “forced” acoustic motion in the contained fluid consists of a decaying pressure field which closely hugs the shell wall. At the $\Omega = 0.56$ the next branch $s = 2$ cuts on, and this branch corresponds to the first rigid walled duct mode with circumferential variation $n = 1$. Due to the slight compliance of the shell wall its phase velocity lies between that of a rigid walled and a pressure release mode.

At $\Omega = 0.7$ a third branch, $s = 3$, with predominantly torsional shell motion cuts on. This branch continues to behave in a torsional manner until it encounters branch $s = 4$ where its characteristics change to a fluid-type wave. Thus for higher circumferential modes ($n > 1$) there are two series of plateaux arising from coincidence of torsional and extensional shell waves with duct type waves.

As well as the complex branches already demonstrated in the case of the $n = 0$ mode, there appears, in the case of the $n = 1$ mode, a pair of complex branches near $\Omega = 0.5$ which link together the branches $s = 2$ and $s = 3$ in the evanescent region, and further illustrate coincidence behaviour of waves below cut-off. As the slope of the dispersion curves are not vastly different for the branches $s = 2$ and $s = 3$, coincidence behaviour occurs over a wider frequency range than for propagating waves.

Waves with higher circumferential modal number ($n > 1$) exhibit dispersion characteristics similar to those of the beam mode except that the fundamental shell type wave has a non-zero cut-on frequency and the points of coincidence are shifted to higher frequencies.

4.3. STEEL SHELL OF THICKNESS $h/a = 0.005$

The shell system discussed in this section has the same parameters as in the previous section except that the shell wall thickness is assumed to be much smaller in order to illustrate the dependence of the shape of the dispersion curves on wall thickness. The main effect of a reduction in shell thickness is a decrease in stiffness of the shell structure and a corresponding change in branch shape from behaviour like rigid walled duct modes to approaching pressure release behaviour.

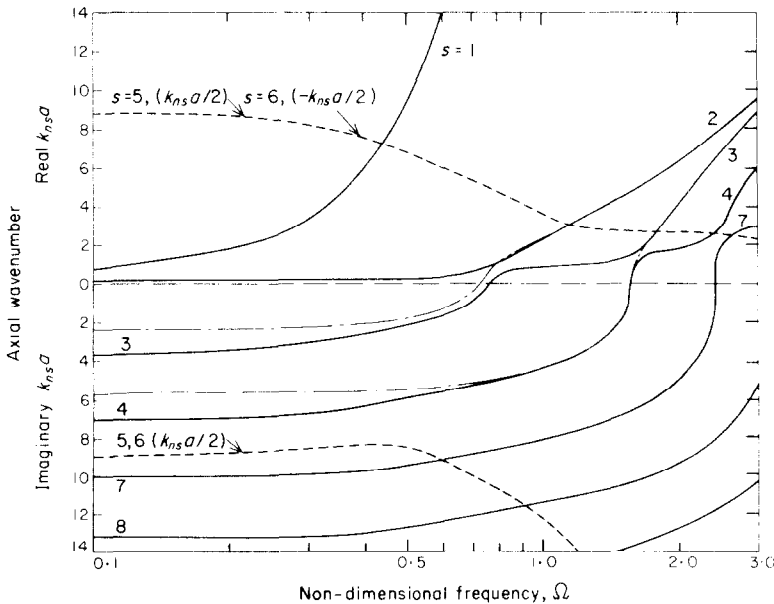


Figure 5. Dispersion curves for a water-filled steel shell of thickness $h/a = 0.005$, $n = 0$; —, purely real and imaginary $k_{ns}a$; ---, real and imaginary parts of complex $k_{ns}a$; - · - ·, pressure release duct solution.

The breathing mode ($n = 0$) response of the system is plotted in Figure 5. In the real plane the $s = 2$ branch has the same form as in the thicker shell shown in Figure 3. The $s = 1$ branch illustrates a marked change. At very low frequencies it is similar to a rigid walled duct mode; however it quickly changes to a shell-type motion with a very small phase speed and low group velocity. This branch represents motion that is acoustically "slow" and is thus mainly uncoupled from the fluid. Thus for shells with very thin walls vibrating in the breathing mode at low frequencies ($\Omega < 0.7$), the energy propagated will be concentrated in the shell wall and mainly carried by the $s = 2$ branch: i.e., in extensional motion. With a further decrease in wall thickness the $s = 1$ branch is found to swing away counter-clockwise to the origin until when $h/a \approx 0$ it would completely disappear and the remaining dispersion curves would represent acoustic waves propagating in a duct with free boundaries combined with the membrane behaviour of the shell.

The purely imaginary branches in Figure 5 are close to rigid walled duct modes at very low frequencies, but quickly approach the evanescent pressure release duct behaviour with increasing frequency. The branches are seen from Figure 5 to transform from rigid walled to pressure release duct solutions near the intersection with the imaginary part of the bending near field branch. It is close to this frequency that the shell becomes more flexible in the radial direction. For very thin shells there are no hooks in the imaginary branches due to the decrease in influence of bending stiffness of the shell wall relative to the fluid motion. Likewise the complex branches $s = 5$ and 6, which are very close to *in vacuo* shell branches at very low frequencies, do not intersect the imaginary plane (in the frequency range of this analysis). Hence the near field coincidence behaviour observed for the thicker shell ($h/a = 0.05$) does not occur for the thinner shell discussed here. With decreasing wall thickness, the complex branches are found to increase in absolute magnitude, and swing clockwise relative to the origin, until, when $h/a \approx 0$, they disappear.

Dispersion branches for the $n = 1$ beam mode for the same shell are presented in Figure 6. As in the case of the $n = 0$ mode, the reduction in wall thickness results in a

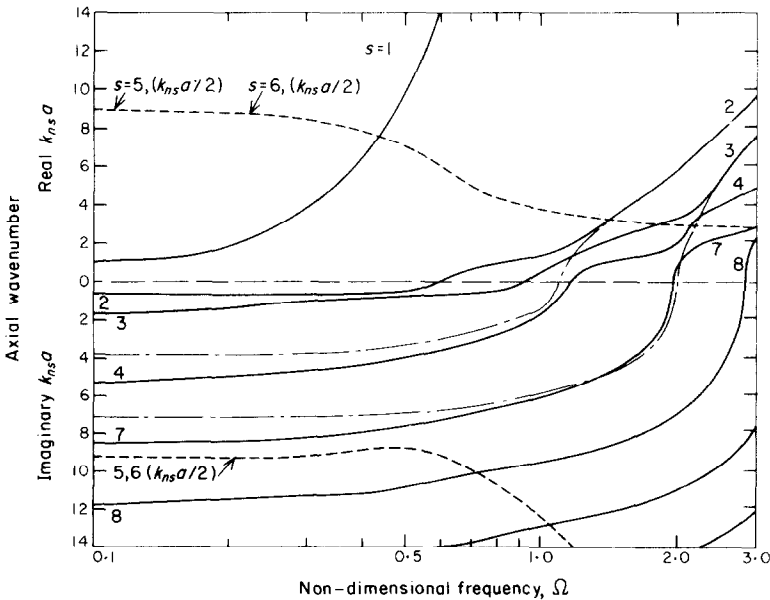


Figure 6. Dispersion curves for a water-filled steel shell of thickness $h/a = 0.005$, $n = 1$; —, purely real and imaginary $k_{ns}a$; ---, real and imaginary parts of complex $k_{ns}a$; - · - ·, pressure release duct solution.

general change towards pressure release duct behaviour. In the real plane the $s = 1$ branch is close to the *in vacuo* beam branch at low frequencies, but its phase and group velocities decrease sharply with increasing frequency and it correspondingly becomes increasingly decoupled from the fluid field. Below cut-on the next branch, $s = 2$, is, for the thinner shell, a torsional type motion which changes to a pressure release wave at higher frequencies. The $s = 3$ branch represents the first fluid-type duct wave to cut on; however, soon after its inception it transfers into a torsional type motion in the manner discussed previously, and then, at higher frequencies, approaches the second pressure release solution.

The imaginary and complex branches of the beam mode exhibit the same general changes in behaviour with reduction in wall thickness as seen for the breathing mode. In particular, the complex root linking the $s = 2$ and $s = 3$ branches near cut-on has disappeared. Very thin fluid-filled shells can thus be seen from Figure 6 generally to support no wave motion (in terms of propagation of energy) in the $n = 1$ mode until the inception of the first stretching type of shell wave, the torsional mode. Very thin shells also exhibit no evanescent coincidence behaviour as shown in the behaviour of thicker shells.

4.4. HARD RUBBER SHELL OF THICKNESS $h/a = 0.05$

For this example the cylindrical shell was assumed to be constructed of hard rubber of wall thickness $h/a = 0.05$, with material properties given in Table 1. As rubber has a much lower extensional free wave speed than steel, the acoustic modes for a hard rubber shell filled with water will not cut on until a much higher value of non-dimensional frequency Ω is reached (see equation (9)) than for a water-filled steel shell of the same dimensions. Consequently the behaviour of the dispersion of waves in rubber shells filled with water is significantly different from the behaviour discussed in the previous sections.

Curves obtained for the $n = 0$ circumferential mode are presented in Figure 7. At very low frequencies there again occur two branches $s = 1$ and $s = 2$ in the real plane which

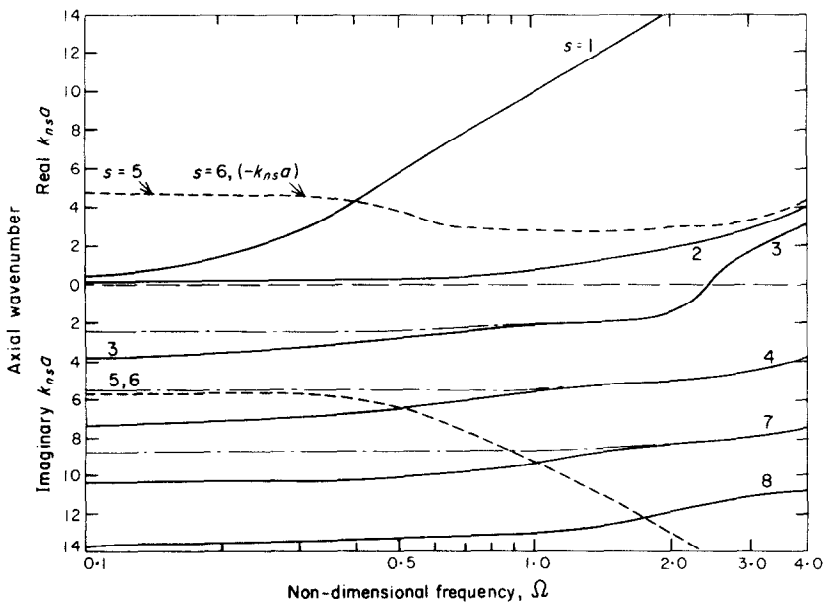


Figure 7. Dispersion curves for a water-filled hard rubber shell of thickness $h/a = 0.05$, $n = 0$; —, purely real and imaginary $k_{ns}a$; ---, real and imaginary parts of complex $k_{ns}a$; - · -, pressure release duct solution.

respectively behave as a rigid walled acoustic plane wave and an extensional shell wave largely decoupled from the fluid. As the frequency is increased, the $s = 1$ branch quickly changes its characteristics to those of a shell-type wave which is acoustically "slow". The $s = 2$ branch, contrary to steel shell behaviour, remains purely extensional throughout the frequency range. In the example discussed here, the fluid resonances (or cut-on) do not occur until a much higher frequency. Thus for $\Omega \leq 2.5$ the fluid appears to have a high impedance relative to the shell wall and constrains the motion of the shell wall to vibrations in the axial plane. Similarly the high impedance of the acoustic field in the contained fluid suppresses the cut-on of the $n = 0$ extensional shell type wave near $\Omega = 1.0$. This mode, in the case of an *in vacuo* shell, has purely radial amplitude at cut-on, and is thus prevented from propagating.

At $\Omega = 2.48$ a third branch, $s = 3$, occurs which initially behaves like a duct wave in a slightly compliant tube, and then quickly approaches the first pressure release type mode. With increasing frequency more waves cut on as pressure release waves. Due to the fact that the extensional wave speed of free motion in the rubber is slower than for free acoustic waves, the fluid type branches of Figure 7 do not intersect any shell type branches and the plateaux observed in the case of steel shells in Figures 3-6 are absent from Figure 7. Thus for fluid-filled shells with a phase speed ratio such that $c_L/c_f < 1$, coincidence between shell and fluid response will not occur. This result has important implications in terms of sound radiation and transmission losses of cylindrical shells.

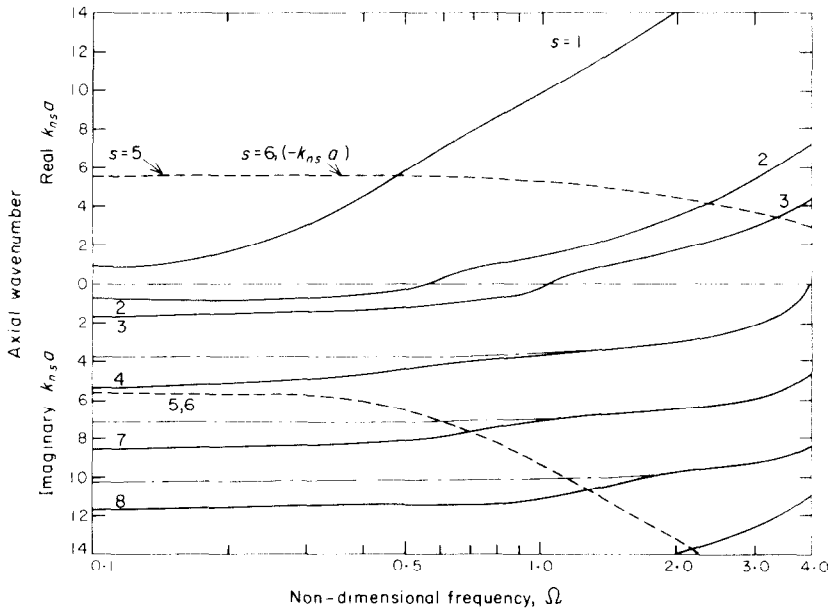


Figure 8. Dispersion curves for a water-filled hard rubber shell of thickness $h/a = 0.05$, $n = 1$: —, purely real and imaginary $k_{ns}a$; ---, real and imaginary parts of complex $k_{ns}a$; - · - ·, pressure release duct solution.

Dispersion curves for the $n = 1$ mode, plotted in Figure 8, demonstrate effects similar to those of the $n = 0$ mode for a change in wall material, except for the $s = 2$ branch, which is largely unaffected by the fluid. The $s = 2$ branch cuts on as a torsional type wave and remains purely torsional throughout the frequency range. The torsional shell wave has a large axial amplitude at cut-on, which changes to a large torsional amplitude at high frequencies; its behaviour is thus unchanged by the presence of the fluid. The $s = 3$ branch cuts on as an extensional shell type wave. All higher modes behave like

pressure release duct modes ($\Omega \gg 1$), and like the $n = 0$ mode there are no coincidence points, or plateaux, in the dispersion branches.

5. ENERGY DISTRIBUTIONS IN FLUID-FILLED SHELLS

When waves propagate through fluid-filled piping systems there will be a distribution of energy of vibration between the pipe wall and the contained fluid. The degree to which the energy is concentrated in the fluid or the shell wall will depend upon the type of excitation of the piping system and the physical parameters of the shell and the contained fluid. In the interests of effecting noise control and vibration reduction, it is of prime importance to be able to predict the distribution of energy in vibrating shells. Thus, in this section, an exact equation is developed which gives the ratio of the energy fluxes in the shell and fluid for a particular mode travelling in a fluid-filled shell. In a practical situation there will be many modes excited by the driving source: however, the following analysis provides a first step to a detailed understanding of energy distributions in forced vibration of piping systems.

5.1. POWER FLOW IN THE FLUID FIELD

The fluid field is assumed to obey the acoustic wave equation for small vibrations and it can thus be described by the usual pressure solution in cylindrical co-ordinates for a particular mode (n, s),

$$p = P_{ns} \cos(n\theta) J_n(k_s^r r) \exp[i\omega t - ik_{ns} x]. \quad (10)$$

The axial acoustic particle velocity can be obtained from the momentum relation,

$$v_x = -(1/i\rho_f \omega) \partial p / \partial x \quad (11)$$

and thus the axial velocity is,

$$v_x = (k_{ns}/\rho_f \omega) P_{ns} \cos(n\theta) J_n(k_s^r r) \exp[i\omega t - ik_{ns} x]. \quad (12)$$

Acoustic power flux density, or intensity, in the axial direction is given by

$$I(\theta, r, t) = \frac{1}{2} \text{Real}(p \bar{v}_x), \quad (13)$$

where \bar{v} is the complex conjugate of v . Thus axial intensity is

$$I(\theta, r, t) = (P_{ns}^2/2)(k_{ns}/\rho_f \omega) \cos^2(n\theta) J_n^2(k_s^r r), \quad (14)$$

where P_{ns} is assumed to be a real amplitude.

The total power is obtained by integrating the intensity given by equation (14) flowing through an element of area $dS = r d\theta dr$ over the cross-sectional area of the fluid field. Thus total power P_f is

$$P_f = \int_0^{2\pi} \int_0^a I(\theta, r, t) dS = \int_0^{2\pi} \int_0^a \frac{P_n^2}{2} \frac{k_{ns}}{\rho_f \omega} \cos^2(n\theta) J_n^2(k_s^r r) r d\theta dr \quad (15, 16)$$

$$= \pi P_0^2 \frac{k_{0s}}{\rho_f \omega} \int_0^a J_0^2(k_s^r r) r dr \quad \text{for } n = 0 \quad (17)$$

$$= \frac{\pi}{2} P_n^2 \frac{k_{ns}}{\rho_f \omega} \int_0^a J_n^2(k_s^r r) r dr \quad \text{for } n > 0. \quad (18)$$

5.2. POWER FLOW IN THE SHELL WALL

The total axial power flow in the shell wall for a particular radial amplitude has been derived previously [11] and due to the Poisson's coupling effect is the sum of three

individual powers,

$$P_s = P_b + P_a + P_t, \quad (19)$$

where the subscripts refer to the type of shell motion: i.e., in flexure, extension or torsion. P_b consists of two parts contributed by rotation and flexure of the shell element. In equation (19) the individual powers are given by

$$P_b = \int_0^{2\pi} [\frac{1}{2}M_x \dot{\bar{w}}_x + \frac{1}{2}Q_x \dot{\bar{w}}] a \, d\theta, \quad P_a = \frac{1}{2} \int_0^{2\pi} N_x \dot{\bar{u}} a \, d\theta, \quad P_t = \frac{1}{2} \int_0^{2\pi} N_{x\theta} \dot{\bar{v}} a \, d\theta, \quad (20-22)$$

where M_x , θ_x , N_x and $N_{x\theta}$ are the bending moment in the x direction, transverse shear force, axial force and torsional shear force respectively and an overdot implies differentiation with respect to time.

Using the simplified Flügge equations and the displacement distributions assumed in equations (1), one arrives at the total shell power flow for a particular mode (n, s) as [11],

$$P_s = [\pi E (h/a)^3 / 6(1-\nu^2)] \omega a W_{0s}^2 [(k_{0s}a)^3 + R_a (k_{0s}a)^2] + [\pi E (h/a) / (1-\nu^2)] \omega a W_{0s}^2 [(k_{0s}a) R_a^2 + \nu R_a], \quad n = 0, \quad (23)$$

$$P_s = [\pi E (h/a)^3 / 12(1-\nu^2)] \omega a W_{ns}^2 [(k_{ns}a)^3 + \nu n^2 (k_{ns}a) + R_a (k_{ns}a)^2 + n R_t (k_{ns}a)] + [\pi E (h/a) \omega a / 2(1-\nu^2)] W_{ns}^2 [(k_{ns}a) R_a^2 + n \nu R_a R_t + \nu R_a] + (\pi/4) [E (h/a) \omega a (1-\nu) / (1-\nu^2)] W_{ns}^2 [n R_a R_t + (k_{ns}a) R_t^2], \quad n > 0, \quad (24)$$

where in equations (23) and (24) E is the Young's modulus of the shell material and R_a and R_t are the ratios of axial and torsional to radial amplitudes of vibration obtained by re-substituting the derived axial wavenumbers, $k_{ns}a$, back in the matrix of system equations (5).

5.3. POWER FLOW IN THE COUPLED SYSTEM

As shown in section 2, by application of the boundary condition at the shell wall of continuity of radial fluid and shell velocity, the fluid power can be written in terms of the shell radial amplitude of vibration, W_{ns} . Substituting equation (4) into equations (17) and (18) gives

$$P_f = \pi \omega^3 k_{0s} \rho_f [k_s' J_0'(k_s' a)]^{-2} W_{0s}^2 \int_0^a J_0^2(k_s' r) r \, dr, \quad n = 0, \quad (25)$$

$$P_f = (\pi/2) \omega^3 k_{ns} \rho_f [k_s' J_n'(k_s' a)]^{-2} W_{ns}^2 \int_0^a J_n^2(k_s' r) r \, dr, \quad n > 0. \quad (26)$$

The ratio of power flow or (as group velocity is the same for both media) energy distribution between the fluid and shell vibrational field is thus given by

$$E_r = P_f / P_s = \omega^3 k_{ns} \rho_f [k_s' J_n(k_s' a)]^{-2} \int_0^a J_n^2(k_s' r) r \, dr / [E / (1-\nu^2)] \omega a S_f, \quad (27, 28)$$

where the shell factor S_f is

$$S_f = [(h/a)^3 / 6] [(k_{ns}a)^3 + \nu n^2 (k_{ns}a) + R_a (k_{ns}a)^2 + n R_t (k_{ns}a)] + (h/a) [(k_{ns}a) R_a^2 + n \nu R_a R_t + \nu R_a] + [(h/a) / 2] (1-\nu) [n R_a R_t + (k_{ns}a) R_t^2]. \quad (29)$$

The integral in equation (28) takes the form of Lommel's integral, the solution of which

can be written as [14]

$$\int_0^a r J_n^2(k'_s r) dr = \frac{a^2}{2} \left\{ [J'_n(k'_s a)]^2 + \left(1 - \frac{n^2}{(k'_s a)^2} \right) J_n^2(k'_s a) \right\}. \quad (30)$$

Substituting equation (30) into equation (28) gives the energy ratio as

$$E_r = \omega^2 \frac{\rho_s}{[E/(1-\nu^2)]} a^2 [k'_s a J_n(k'_s a)]^{-2} (k_{ns} a) \frac{\rho_f F_f}{\rho_s S_f}, \quad (31)$$

where F_f is the fluid factor given by

$$F_f = \frac{1}{2} \{ [J'_n(k'_s a)]^2 + [1 - n^2 / (k'_s a)^2] J_n^2(k'_s a) \}. \quad (32)$$

Equation (31) can be further simplified by the substitution of $c_L^2 = E/[\rho_s(1-\nu^2)]$ and $\Omega = \omega a / c_L$, to give the final non-dimensional relationship for energy distribution,

$$E_r = \Omega^2 (\rho_f / \rho_s) (k_{ns} a) [k'_s a J'_n(k'_s a)]^{-2} (F_f / S_f). \quad (33)$$

The energy ratio given by equation (33) can be evaluated by substituting in the appropriate values of axial and radial wavenumbers obtained previously. Figures 9(a) and (b) show typical energy ratios for normal propagating modes in a steel shell of thickness of $h/a = 0.05$ filled with water for the $n = 0$ and $n = 1$ modes respectively.

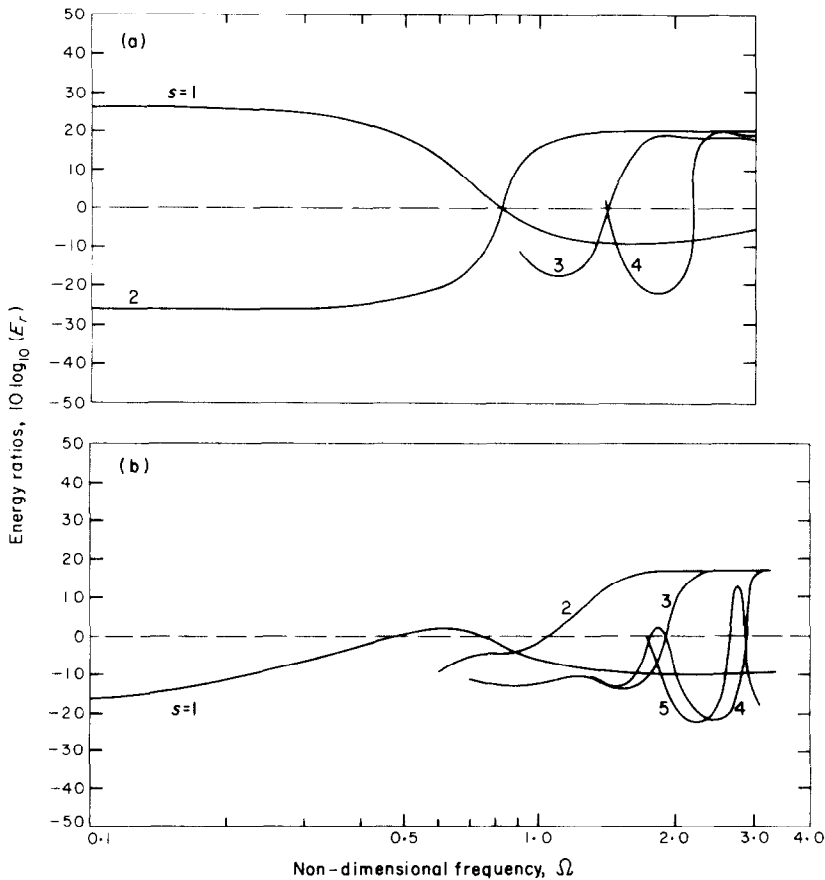


Figure 9. Distribution of vibrational energy in a water-filled steel shell of thickness $h/a = 0.05$. (a) $n = 0$; (b) $n = 1$.

Inspection of equation (33), with reference to Figures 9(a) and (b), gives immediate insight into the distribution of vibrational energy in fluid-filled shells. At low frequencies ($\Omega < 1.0$) for the $n = 0$ mode the majority of energy can be seen to be either in the shell or the fluid depending upon whether the excitation is structural or located in the fluid. As intuitively expected, decreasing the ratio ρ_f/ρ_s , or increasing the ratio h/a , decreases the proportion of energy contained in the fluid for shell type waves. On the other hand, similar parameter changes will cause an increase in energy content in the fluid for fluid type waves, due to the fact that $J'_0(k'_s a)$ approaches zero (the fluid waves approach rigid-walled modes). Thus for $n = 0$ modes, when the shell wall is relatively thick ($h/a \geq 0.01$), or relatively dense ($\rho_f/\rho_s \ll 1$), the energy will be carried predominantly either in the fluid, or in the shell wall, depending upon the form of excitation. When the shell wall is relatively thin ($h/a \leq 0.01$) or less dense ($\rho_f/\rho_s \geq 1$) at low frequencies the energy will nearly all be present in the shell wall.

At high frequencies when higher order fluid-type waves cut on, the energy may be distributed to a varying degree between the shell and fluid. Figure 9(a) illustrates the change in behaviour of the branch $s = 2$ (see Figure 3), which is close to a shell wave at low frequencies, and like a fluid wave at high frequencies. In Figure 4(a) the energy ratio for the $s = 2$ branch can be seen to change sharply near $\Omega = 0.8$, where the shell resonates as a ring. Similarly the fluid branch, $s = 1$, changes into a shell-type wave at the same frequency. At $\Omega = 0.8$ the ratio of energy flux in both branches is close to unity, and as both the fluid and shell fields resonate in the radial direction there is an equal distribution of energy in the media. Thomson's analysis [5], which predicts the $s = 1$ but not the $s = 2$ branch, and neglects certain shell energy flux terms, also indicates a shift of energy from the fluid to the shell at frequencies in the range $\Omega = 1$ to 4 (note in reference [5] $\Omega = \omega a/c_f$). The energy ratios of the higher modes are interesting because they demonstrate the plateau behaviour observed in the dispersion curves. As the higher modes cut on, the energy is predominantly in the fluid, shifts to the shell wall in a plateau region, and then reverts to the fluid. At the coincidence points discussed previously, the energy ratios of the two branches are both equal and close to unity; hence there is uniform distribution of energy between the shell and the fluid at coincidence. The energy ratios of Figure 4(a) also reveal that the $s = 1$ and $s = 2$ branches exhibit coincidence behaviour at $\Omega \approx 0.82$, a result not observable in the corresponding dispersion curve shown in Figure 3.

The energy ratios for modes in fluid-filled shells vibrating in the $n = 1$ or beam mode are given in Figure 9(b). At low frequencies (Ω less than the first cut-on frequency of the fluid-type waves) the energy of vibration is nearly all in the shell wall carried by the wave corresponding to the $s = 1$ branch of Figure 4. With increasing frequency the energy ratio of the $s = 1$ branch increases until at $\Omega = 0.6$ there is more energy in the fluid than the shell wall. This result is surprising since the radial wavenumber of the $s = 1$ branch is imaginary and the fluid motion consists of a "forced" pressure field near the shell wall. However, at $\Omega \approx 0.6$ the radial amplitude of motion of the shell wall is substantially greater than the corresponding motion of the shell *in vacuo*, and as this frequency is close to the cut-on frequency of the first fluid wave, the "forced" pressure amplitude in the fluid is very high. Thus, although the $s = 1$ branch is essentially a beam mode, for the frequency range $0.5 < \Omega < 0.7$ there will be more energy in the "forced" fluid motion. Contrary to the behaviour for other waves with a greater concentration of energy in the fluid, a reduction in shell vibration will have a marked effect on the fluid response due to its "forced" nature. At higher frequencies the energy shifts back to the shell wall for the $s = 1$ branch due to a reduction in "forced" pressure amplitude.

For all other branches occurring at higher frequencies the energy may be predominantly in the shell wall or in the fluid, depending upon the branch and thus on the nature of

the excitation. The curves for the $n = 1$ mode exhibit the double plateau response shown in the dispersion curves, i.e., the energy shifts from the fluid to the shell in two frequency regions, and thus there are two coincidence points for a branch where coupling occurs between torsional or axial shell waves and fluid waves.

On the whole, the energy curves demonstrate that fluid-filled cylindrical shells will vibrate in dominantly fluid or shell-type motion except at a number of discrete coincidence frequencies where the vibrational energy is shared equally.

6. CONCLUSIONS

The dispersion and energy distributions of free waves in fluid-filled cylindrical shells has been examined. The behaviour of individual branches has been explained for a variation in parameters. The behaviour of free waves is found to depend strongly upon the thickness of the shell wall, and on the ratio of the density of the shell material to the density of the contained fluid. Coincidence behaviour for propagating and evanescent waves has been identified and explained. An exact equation which predicts energy distribution in fluid-filled shells has been developed and its parametric variation studied. Generally, at low frequencies most of the energy is concentrated in the shell wall for structural excitation. For acoustical excitation at low frequencies the energy is predominantly in the fluid. At higher frequencies the energy may be in the fluid field or in the shell wall.

ACKNOWLEDGMENTS

The authors gratefully acknowledge the Ministry of Defence for supporting this work.

REFERENCES

1. H. LAMB 1898 *Manchester Literary and Philosophical Society—Memoirs and Proceedings* **42**(9). On the velocity of sound in a tube, as affected by the elasticity of the walls.
2. R. D. FAY, R. L. BROWN and O. V. FORTIER 1947 *Journal of the Acoustical Society of America* **19**, 850–856. Measurement of acoustic impedances of surfaces in water.
3. W. J. JACOBI 1949 *Journal of the Acoustical Society of America* **21**, 120–127. Propagation of sound waves along liquid cylinders.
4. M. A. BIOT 1952 *Journal of Applied Physics* **23**, 997–1005. Propagation of elastic waves in a cylindrical bore containing a fluid.
5. W. T. THOMSON 1953 *Proceedings of the First U.S. National Congress on Applied Mechanics, Chicago*, 922–933. Transmission of pressure waves in liquid filled tubes.
6. T. C. LIN and G. W. MORGAN 1956 *Journal of the Acoustical Society of America* **28**, 1165–1176. Wave propagation through fluid contained in a cylindrical, elastic shell.
7. R. KUMAR 1972 *Acustica* **27**, 317–329. Dispersion of axially symmetric waves in empty and fluid-filled cylindrical shells.
8. V. N. MERKULOV, V. YU. PRIKHODKO and V. V. TYUTEKIN 1978 *Soviet Physics—Acoustics* **24**, 405–409. Excitation and propagation of normal modes in a thin cylindrical elastic shell filled with fluid.
9. P. H. WHITE and R. J. SAWLEY 1972 *Trans. A.S.M.E., Journal of Engineering for Industry* **94**, 746–751. Energy transmission in piping systems and its relation to noise control.
10. M. C. JUNGER and D. FEIT 1972 *Sound, Structures and Their Interaction*. Cambridge, Massachusetts: M.I.T. Press.
11. C. R. FULLER 1981 *Journal of Sound and Vibration* **75**, 207–228. The effects of wall discontinuities on the propagation of flexural waves in cylindrical shells.
12. F. S. ACTON 1970 *Numerical Methods that Work*. New York: Harper and Row.
13. R. KUMAR and R. W. B. STEPHENS 1972 *Proceedings of the Royal Society of London* **A329**, 283–297. Dispersion of flexural waves in circular cylindrical shells.
14. N. W. MCLACHLAN 1934 *Bessel Functions for Engineers*. London: Oxford University Press.

APPENDIX: LIST OF SYMBOLS

a	thin shell mean radius
c_f	fluid acoustic free wave speed
c_L	shell extension phase speed
E	Young's modulus
E_r	energy ratio
F_f	fluid factor
FL	fluid loading term
h	shell wall thickness
I	intensity
i	$\sqrt{-1}$
$J_n(\)$	Bessel function of order n
k_{ns}	axial wavenumber
k'_r	radial wavenumber
M_x	bending moment in the x direction around tangential axis
N_x	axial force
$N_{x\theta}$	torsional shear force
p	pressure
P_f	power flow in fluid
P_s	power flow in shell
P_{ns}	pressure amplitude
Q_x	transverse shear force
r	cylindrical co-ordinate
R_a	ratio of axial to radial amplitude of shell motion
R_r	ratio of torsional to radial amplitude of shell motion
s	branch number
S	area
S_f	shell factor
u, v, w	shell displacements
U_{ns}, V_{ns}, W_{ns}	shell displacement amplitudes
x	cylindrical co-ordinate
v_a	acoustic axial particle velocity
v_r	acoustic radial particle velocity
Z	wall impedance
β	thickness factor
θ	cylindrical co-ordinate
ρ_f	density of fluid
ρ_s	density of shell
ν	Poisson's ratio
ω	circular frequency
Ω	non-dimensional frequency
$(\)$	complex conjugate
$(\)$	differentiation with respect to time
$(\)$	differentiation with respect to $k'_r r$